JOURNAL OF COMPUTATIONAL PHYSICS 30, 107–124 (1979)

# Boundary-Fitted Coordinates for Accurate Numerical Solution of Multibody Flow Problems

H. J. HAUSSLING

*David W. Taylor Naval Ship Research and Development Center, Bethesda, Maryland 20084*

Received October 11, 1977; revised January 20, 1978

A transformation is presented which maps an arbitrary two-dimensional region of connectivity $N$ into $N - 1$ simply connected regions composed of rectangles. Uniform grids are used in the transformed regions to yield finite-difference meshes which are suitable for the accurate numerical solution of multibody flow problems. The utility of the transformation is verified with its application to the Weis-Fogh mechanism of lift generation.

## INTRODUCTION

The numerical generation of boundary-fitted coordinate systems, specifically coordinate systems generated from elliptic partial differential equations, has recently been shown to be a powerful tool for use in the finite-difference solution of fluid flow problems. The first work which adequately exposes the potential of these coordinate systems is that of Thompson, Thames, and Mastin [1]. However, this early work—in fact, even the progress which has been made since then—only begins to exercise the capabilities of these methods.

For example, the transformations used in [1] were defined by solutions to the Laplace equation. Experience with such transformations shows that one has very little control over the resulting finite-difference meshes, making optimum spatial distribution of grid points difficult to achieve. In more recent work described by Thompson *et al.* [2] Poisson equations are used to generate the transformations. Specification of the source terms in the Poisson equations provides added control over the grid generation. Specific expressions for the source terms were suggested by Thompson *et al.* [3], and Ghia, Ghia, and Studerus [4] have carried out some research on the choice of source terms to generate a grid with desirable properties. However, more research is needed in this area to develop the capability of easily generating grid systems with efficient distributions of points for a wide variety of flow problems.

In addition to the form of the generating equations, the shape of the computational region into which the physical region is mapped influences the shape of the mesh in physical space. In [1] a doubly-connected flow region was mapped onto a rectangle with one side formed by the body surface. The restriction to such a transformed region is quite limiting, although the resulting grids are adequate for a body in an infinite fluid. Thompson *et al.* [3] presented a transformation in which a body is mapped to a



0021-9991/79/010107-18$02.00/0

slit within a rectangle. This procedure can be useful when resolution is important near one or more of the exterior flow boundaries. By mapping into a region consisting of two adjoining rectangles Thompson *et al.* [2] demonstrated a transformation which is useful for concentrating large numbers of grid points in the neighborhood of the body. This idea was carried one step further by Haussling and Coleman [5] with a transformation for flow about a body below a free surface onto an H-shaped computational region.

Recently there has been much interest in the application of the finite-element method to fluid flow problems (see, for instance, Connor and Brebbia [6]). One reason for this interest is the finite-element capability for efficiently fitting complicated geometries. However, the development of numerically generated coordinate systems gives such a relatively easy to use capability to finite-difference schemes even for time-dependent geometries.

The presentation of a variety of transformed regions as mentioned above serves to extend the flexibility of these coordinate system generation techniques. The present paper is intended to further demonstrate this flexibility in application to multibody problems. Thompson *et al.* [3] described how flow regions involving multiple bodies could be handled by transformations onto rectangles or slit rectangles. While such transformations may be adequate for some problems, in other cases they cannot provide efficient grid point distributions. With both of these transformations, grid points cannot be added near the bodies without also adding grid points to the mesh in the far field. Recently Long [7], using these methods, had difficulties in obtaining suitable coordinate systems for some two-body problems. He resorted to the use of an additional complex variable transformation. This paper describes a new type of multibody transformation which has some desirable properties for optimum grid point distribution. It should extend the class of problems which can be handled by the elliptic generating system approach. The workability of the transformation is verified with its application to the Weis-Fogh mechanism of lift generation [8, 9].

## The Multibody Transformation

It has long been recognized that, in studying flows about a single body, the use of a cylindrical coordinate system often results in an efficient finite-difference scheme. The grid expands naturally with distance from the body and the rate of expansion can be varied by additional grid stretching. Such a coordinate system for an arbitrary body can be generated numerically as shown by Thompson, Thames, and Mastin [1].

When the flow about more than one body is considered, it would sometimes be useful to have a coordinate system which is locally cylindrical about each body individually but which in the far field is cylindrical about the collection of bodies. This scheme allows grid points to be concentrated near the bodies without using an undue number of points in the far field. Such a transformation will now be described. For simplicity, the details will be presented for two bodies; extension to more than two is straightforward.

Consider two bodies of arbitrary shape as represented in Fig. 1a. The bodies are enclosed by a computational outer boundary. Cuts (dashed lines) are made from A′/B′ to A/B and from E/E′ to F/F′. The triply-connected physical region in $(x, y)$-space is to be mapped to the two simply-connected computational regions in $(\xi, \eta)$-space as shown in Fig. 1b. The boundary of each computational region consists of the images of one of the bodies, half of the outer boundary, and portions of the cuts.

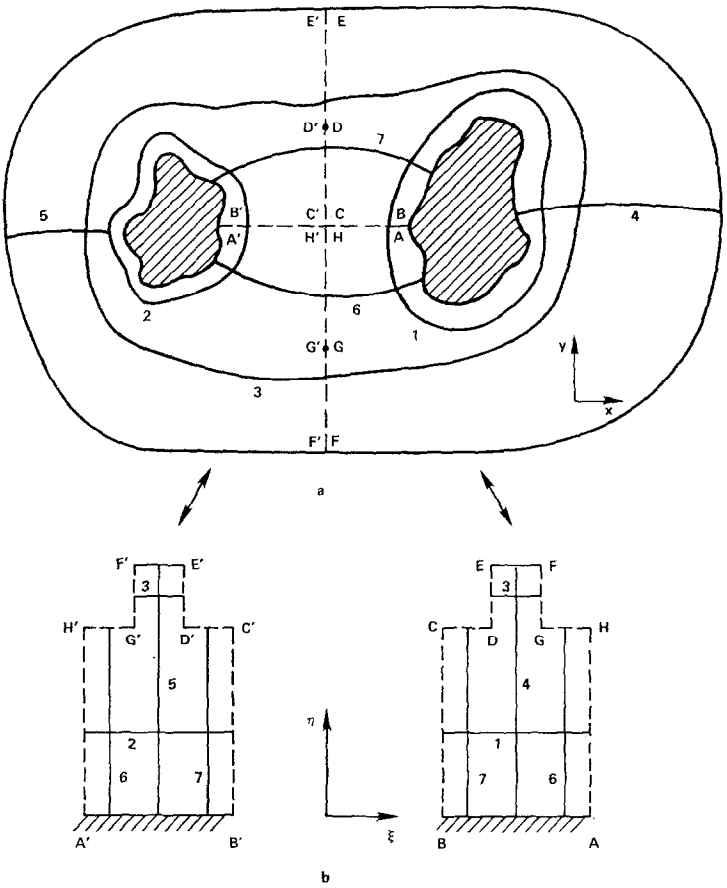


FIG. 1. The field transformation for two Bodies: (a) physical region, (b) computational regions.

A uniform grid is laid out in the computational regions. A grid line such as 1, which extends from AH to BC in the computational region, is to surround the body AB in physical space. Similarly, grid line 2 will surround body A′B′. Grid line 3, which extends in the computational plane in two segments from FG to DE and from D′E′ to F′G′, will surround the pair of bodies. Grid lines such as 4 and 5 will extend from the bodies to the outer boundaries. Lines such as 6 and 7, each of which is split into two segments in the computational region, will connect the two bodies.

The two computational regions will be of different size unless the number of grid points on each body and the number of grid lines surrounding each body is the same. The transformation will depend on time $t$ if the relative position of the bodies changes with time. The transformation is singular at the points D/D′ and G/G′ so that care will be needed in the finite-difference treatment of the neighborhood of these points. The existence of such singularities is not confined solely to this type of mapping. They occur whenever a smooth line such as CDE in Fig. 1a is mapped to a configuration with a corner such as CDE in Fig. 1b. The two-body transformations presented by Thompson *et al.* [3] also contain such singularities but in those cases they are at the body surfaces. Thus, if any accuracy problems do arise from such points, the present transformation has an advantage in that the singularities are removed from the body surfaces.

The desired transformation

$$\xi = \xi(x, y, t), \qquad \eta = \eta(x, y, t) \tag{1}$$

can be found as a solution of Poisson equations

$$\begin{aligned} \xi_{xx} + \xi_{yy} &= P(\xi, \eta, t), \\ \eta_{xx} + \eta_{yy} &= Q(\xi, \eta, t) \end{aligned} \tag{2}$$

with appropriate boundary conditions. The details of the coordinate system can be controlled by specification of the source functions $P$ and $Q$. Following standard procedure, the roles of the dependent and independent variables are interchanged to yield

$$\begin{aligned} \alpha x_{\xi\xi} - 2\beta x_{\xi\eta} + \gamma x_{\eta\eta} &= -J^2(x_\xi P + x_\eta Q), \\ \alpha y_{\xi\xi} - 2\beta y_{\xi\eta} + \gamma y_{\eta\eta} &= -J^2(y_\xi P + y_\eta Q), \end{aligned} \tag{3}$$

where

$$\begin{aligned} \alpha &= x_\eta^2 + y_\eta^2, \qquad \beta = x_\xi x_\eta + y_\xi y_\eta, \\ \gamma &= x_\xi^2 + y_\xi^2, \qquad J = x_\xi y_\eta - x_\eta y_\xi. \end{aligned} \tag{4}$$

The system (3) is to be solved in the transformed computational region. The boundary conditions on A′B′ and AB (Fig. 1b) are the specified $(x, y)$-coordinates of the bodies. Similarly the $(x, y)$-coordinates of the outer boundary are specified on EF and E′F′. The remaining boundary conditions apply to the pairs of boundary segments in the computational region which coincide in physical space. The $(x, y)$-coordinates ofAH equal those of BC; similar conditions apply to the boundary pairs A′H′ and B′C′, FGH and F′G′H′, and CDE and C′D′E′. Although the exact solution of (3) subject to these boundary conditions is a formidable problem, an approximate solution can be found easily by solving an appropriate finite-difference approximation to (3) on the uniform mesh of the computational region.

## A Sample Application

The superior hovering performance of certain insects was attributed by Weis-Fogh [8] to a previously unknown mechanism of lift generation. This mechanism was analyzed by Lighthill [9]. In part of his analysis, Lighthill considered the two-dimensional flow about two infinitely long wings. The wings lie side by side initially and then open as each rotates about one end (Fig. 2a). Subsequently the wings separate through oppositely directed horizontal translations (Fig. 2b). To obtain a reasonable numerical solution to the Navier–Stokes equations for such a time-dependent geometry appears to be a difficult problem. However, with the transformation described in the previous section this problem can be attacked. Ultimately the forces on the wings, in particular the generation of lift, can be computed.

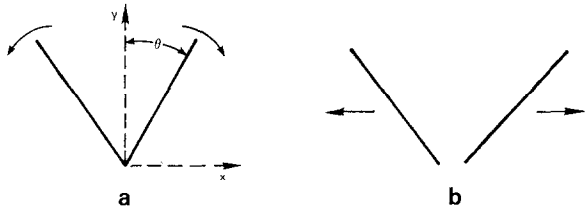


FIG. 2. Wing motions of the Weis-Fogh mechanism.

To demonstrate the feasibility of such a study, some preliminary calculations have been carried out. In order to avoid numerical difficulties associated with treating infinitely thin plates [10], elliptic cylinders with a thickness ratio of 0.01 are used. Since the transformation can be applied only to two distinct bodies, there is a gap between the fixed tips of the plates amounting to about 0.03 chord lengths while they are rotating. The flow for this configuration will be essentially the same as for infinitely thin plates in contact.

Equations (3) and (4) were replaced by finite-difference approximations using second-order central differencing. The finite-difference equations were solved using successive overrelaxation (SOR). The calculations were carried out on a Texas Instruments Advanced Scientific Computer, a vector processor. In the usual SOR procedure each iteration is carried out by updating values at each grid point in turn, for instance by updating all points in natural succession on the first row and then moving from row to row. To accelerate convergence, already updated values at neighboring grid points are used whenever they are available. This use of latest values prohibits vectorization since each step in the calculation cannot be started until the previous step is completed. However, if the mesh is divided into sets of non-adjacent points and relaxed in a series of partial sweeps, in the so-called "red–black" manner, the calculations can be vectorized with no deterioration of convergence rate. Hayes [11] discussed this vectorization for the Laplace equation in rectangular coordinates. She applied the standard SOR scheme in two half-sweeps. For grid points with a standard $(i, j)$ numbering system she alternately updated those with

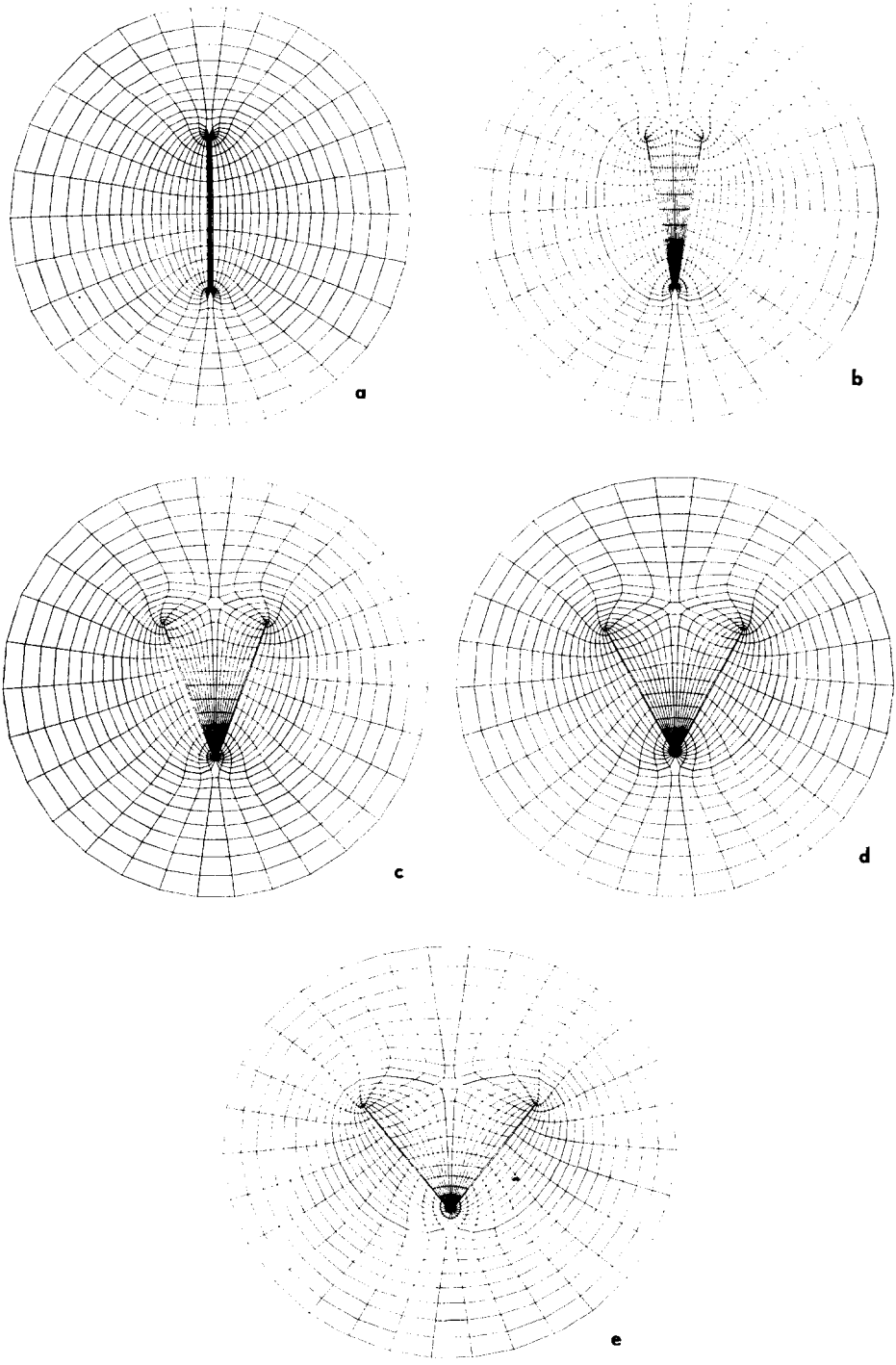
a
b
c
d
e

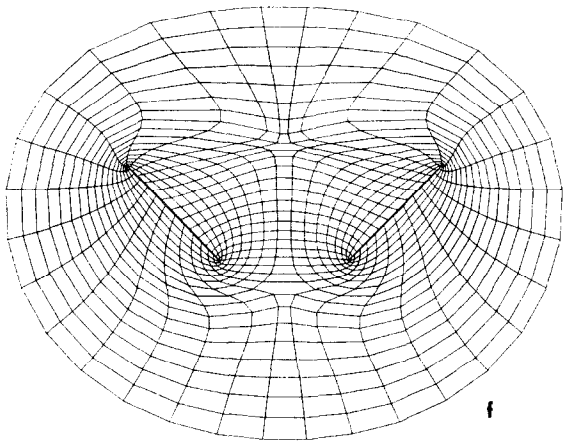


FIG. 3. Meshes for various configurations: (a) $\theta = 0°$, (b) $\theta = 10°$, (c) $\theta = 20°$, (d) $\theta = 30°$, (e) $\theta = 39°$, (f) $\theta = 45°$ and a separation of one chord length.

$i + j$ even and those with $i + j$ odd. Each half-sweep vectorized and the overall scheme was quite efficient. For the present calculations the grid points had to be divided into four groups—defined by the four possible odd–even combinations of $i$ and $j$—since the presence of the cross-derivative terms in Eqs. (3) leads to nine-point finite-difference formulas. It was verified that the desirable properties of this red–black method extend to the mesh generation equations and lead to low execution times.

The near-field grids for various body configurations are presented in Fig. 3a–f. The grid system is composed of 8 lines surrounding each body, 21 lines enclosing the pair, 15 lines extending from each plate to the outer boundary, and 15 lines connecting the plates. A mesh based on a transformation which required all grid lines leaving the bodies to extend to the outer boundary would require at least 56% more grid points in the far field to achieve the same accuracy in the near field. Savings would be even greater for problems with more than two bodies. For the present calculations a further saving results through use of the symmetry about $x = 0$ to limit both the grid generation and fluid flow calculations to one-half of the region.

Grid points are placed on the body surfaces with the aid of local elliptic coordinate systems. The relationship between rectangular coordinates $(x', y')$ and elliptic coordinates $(\eta', \xi')$ for an ellipse with center at $(x' = 0, y' = 0)$ and oriented at an angle $\theta$ to the $x'$, $y'$ system is

$$\begin{aligned} x' &= -\cosh \eta' \cos \xi' \sin \theta + \sinh \eta' \sin \xi' \cos \theta, \\ y' &= -\cosh \eta' \cos \xi' \cos \theta - \sinh \eta' \sin \xi' \sin \theta. \end{aligned} \tag{5}$$

The surface of the ellipse is described by $\eta' = \eta_1$ where $\eta_1$ is the thickness ratio. The grid points on this surface are placed according to

$$\begin{aligned} \eta_j' &= \eta_1, \\ \xi_j' &= \xi_0 + (j - 1)\,\Delta\xi + \theta(t). \end{aligned} \tag{6}$$

The use of equal spacing $\Delta\xi$ in the elliptic system results in concentrations of grid points near the areas of high curvature at the tips of the ellipses. The incorporation of $\theta$ into (6) allows the grid points to slide over the body surfaces as $\theta$ changes with time. If points are fixed to the body surfaces, severe distortions of the grid occur as the bodies move.

The outer boundary is a circle with center at the origin and a radius of about five chord lengths. An outer boundary this close to the bodies might significantly effect force calculations but is sufficient for the demonstration purposes of the present calculations. The uniformly spaced grid points on this boundary are the only points that do not change position with the movement of the plates.

It was found that the use of Laplace equations to generate the transformation is unsuitable. Figure 4 shows a grid generated with such a system. The regions near the points D/D′ and G/G′ (Fig. 1) are poorly resolved. Source terms are needed to pull grid lines toward these points. The source terms take the form

$$\begin{aligned} P(\xi, \eta, t) &= C_1(t)\,\mathrm{sgn}(\xi - \xi_0)\exp\{-[(\xi - \xi_0)^2 + (\eta - \eta_0)^2]^{1/2}\}, \\ Q(\xi, \eta, t) &= C_2(t)\,\mathrm{sgn}(\eta - \eta_0)\exp\{-[(\xi - \xi_0)^2 + (\eta - \eta_0)^2]^{1/2}\} \end{aligned} \tag{7}$$

as suggested by Thompson *et al.* [3] where $(\xi_0, \eta_0)$ are the $(\xi, \eta)$-coordinates of the point to which attraction is desired. The values of the parameters $C_1$ and $C_2$ needed for the generation of suitable meshes were determined experimentally for the configurations of Figs. 3a, e, and f. At other times values of $C_1$ and $C_2$ are assigned by

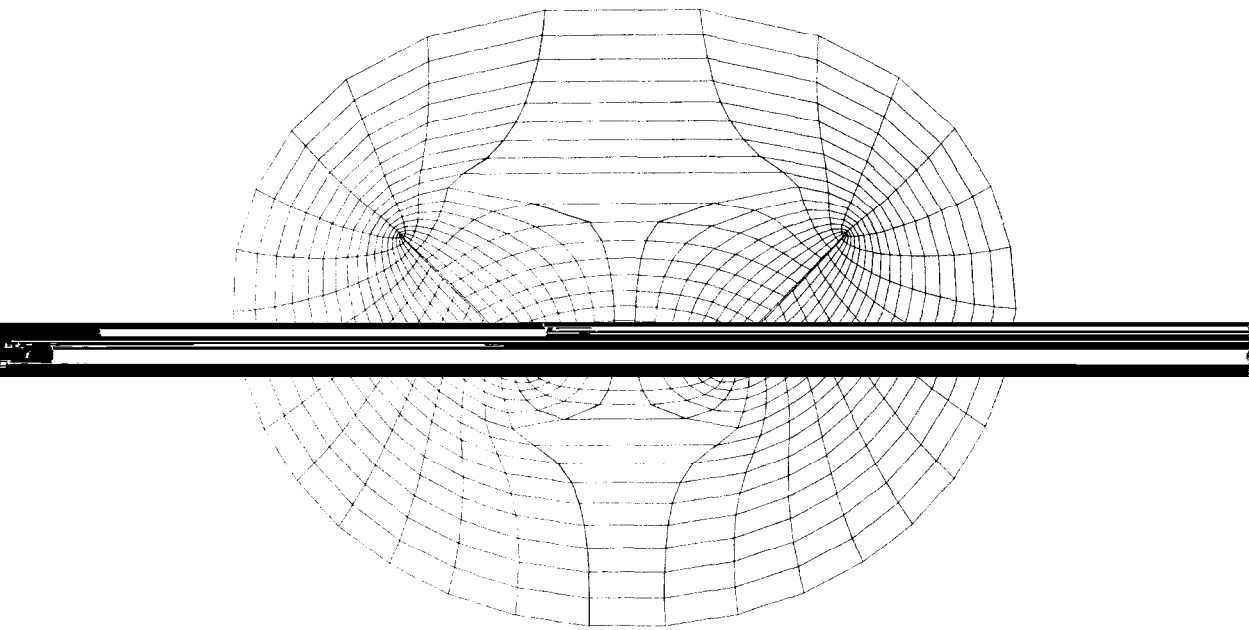

FIG. 4. A Mesh resulting from a transformation generated with Laplace equations.

linear interpolation among the values at these three times. Further improvements might be called for near $\theta = 0°$ (Fig. 3a) when the resolution near the singular points is still somewhat lower than in the surrounding area. The construction of suitable source terms is an important topic of current research. One desirable goal is their automatic generation.

Derivatives in the computational plane are not well defined at points where the transformation is singular such as D/D′ and G/G′. If a grid point is placed at such a location one-sided difference expressions must be employed. To avoid such a complication, grid points were not placed at these locations. As a result two hexagonal cells appear in the grids (Fig. 3). Typical grid point configurations in the vicinity of D/D′ are presented in Fig. 5. An ambiguity arises in the choice of finite-difference operators in such a configuration. Consider a point such as 3 in Fig. 5. The finite-difference approximations to Eqs. (3) will involve eight neighboring points 2, 4, 12, 13, 14, 15, 16, and either 5 or 1. The numerical results should converge to the desired solution

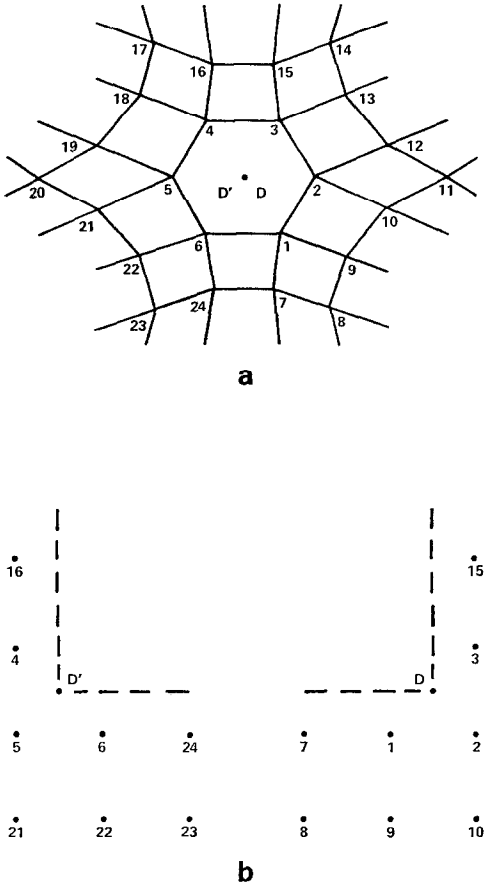


FIG. 5. Grid points near D/D′: (a) physical region, (b) computational regions.

independent of this choice as the mesh is refined. In comparing numerical potential flow solutions with exact solutions the author has yet to find convergence problems associated with such grid regions.

## Viscous Flow Calculations

Two viscous flow computations were carried out. In one, the plates opened and then closed between $\theta = 0°$ and $\theta = 45°$. In the second, after opening to $\theta = 45°$, the plates then separated at constant speed to a separation of about one-half chord. The characteristic length and velocity scales used in defining dimensionless quantities are $a$, the half chord, and $U$ the maximum speed of the tips of the plates. The plate motion for the opening and closing case is defined by

$$\theta(t) = \tfrac{1}{8}\pi[1 - \cos(8t/\pi)], \tag{8}$$

a sinusoidal oscillation starting from $\theta = 0°$ at $t = 0$ and varying between $\theta = 0°$ and $\theta = 45°$. The Reynolds number $\mathrm{Re} = 2Ua/\nu$ is 30 where $\nu$ is the kinematic viscosity. Such a motion involves an alternating acceleration and deceleration. The numerical treatment of various acceleration models was discussed by Lugt and Haussling [12].

The Navier–Stokes equations in dimensionless stream function–vorticity form are

$$\omega_t - \psi_y\omega_x + \psi_x\omega_y = 2(\omega_{xx} + \omega_{yy})/\mathrm{Re}, \tag{9}$$

$$\psi_{xx} + \psi_{yy} = \omega, \tag{10}$$

where $\psi$ is the stream function and $\omega$ is the vorticity.

The boundary conditions on the symmetry line are

$$\psi = \omega = 0 \qquad \text{at } x = 0. \tag{11}$$

Far from the bodies

$$\psi = \omega = 0 \qquad \text{at the outer boundary} \tag{12}$$

and initially

$$\psi = \omega = 0 \qquad \text{at } t = 0. \tag{13}$$

The boundary condition at the body is that the fluid velocity at the body surface equals the velocity of the body or

$$\left.\begin{aligned} \psi_n &= \mathbf{v}_B \cdot \hat{s} \\ \psi_s &= \mathbf{v}_B \cdot \hat{n} \end{aligned}\right\} \qquad \text{at the body surface,} \tag{14, 15}$$

where $\hat{s}$ and $\hat{n}$ are unit vectors in the directions tangential and normal to the body,

respectively, and $\mathbf{v}_B$ is the local velocity of the body surface. Equation (15) can be integrated to yield

$$\psi = \psi_B + c(t) \qquad \text{at the body surface,} \tag{16}$$

where

$$\psi_B = \int \mathbf{v}_B \cdot \hat{n}\, ds. \tag{17}$$

When the plates are essentially in contact the quantity $c$ is chosen such that the stream function is zero at the vertex tips of the plates since these tips are at the symmetry line on which $\psi = 0$ according to (11). After the plates have separated, $c$ must be determined such that the pressure remains single valued. This is done according to the procedure suggested by Sood and Elrod [13]. The pressure $p$ is computed by numerical integration of the momentum equation over the closed body contour. If the value of $c$ is incorrect the pressures at the coincident starting and ending points of the integration will differ. To correct this, an auxiliary problem

$$\psi'_{xx} + \psi'_{yy} = 0, \tag{18}$$

$$\psi' = 0 \qquad \text{at } x = 0, \tag{19}$$

$$\psi' = 0 \qquad \text{at the outer boundary,} \tag{20}$$

$$\left.\begin{aligned} \psi' &= 1 \\ \psi'_n &= \mathbf{v}_B \cdot \hat{s} \end{aligned}\right\} \qquad \text{at the body surface} \tag{21, 22}$$

is solved at each time. The application of the nonslip condition (22) to $\psi'$ implies the existence of a vortex sheet on the surface. An auxiliary multiple-valued pressure $p'$ is computed numerically from this vorticity. Then $c$ is chosen such that the sum of the existing and auxiliary solution $\psi + c\psi'$ results in a single-valued pressure $p + cp'$.

For the calculations, the governing equations and boundary conditions must be transformed to $\xi$, $\eta$-coordinates. Equations (9) and (10) become [3]

$$\begin{aligned} \omega_t = {} & [(\omega_\xi y_\eta - \omega_\eta y_\xi)\, x_t + (\omega_\eta x_\xi - \omega_\xi x_\eta)\, y_t + \psi_\eta \omega_\xi - \psi_\xi \omega_\eta \\ & + 2(\alpha\omega_{\xi\xi} - 2\beta\omega_{\xi\eta} + \gamma\omega_{\eta\eta} + \sigma\omega_\eta + \tau\omega_\xi)/\mathrm{Re}\, J]\, J^{-1}, \end{aligned} \tag{23}$$

$$\alpha\psi_{\xi\xi} - 2\beta\psi_{\xi\eta} + \gamma\psi_{\eta\eta} + \sigma\psi_\eta + \tau\psi_\xi = J^2\omega, \tag{24}$$

where

$$\sigma = J^2 Q, \qquad \tau = J^2 P. \tag{25}$$

The time derivatives in (23) are local derivatives for fixed $(\xi, \eta)$. The terms involving time derivatives on the right-hand side of this equation are required by the time variation of the $(x, y)$-coordinates of points in the $(\xi, \eta)$-plane.

The normal derivative of $\psi$ at a boundary can be written in the form [1]

$$\psi_n = [\psi_\xi(g' y_\eta + x_\eta) - \psi_\eta(g' y_\xi + x_\xi)]/[J(1 + (g')^2)^{1/2}], \tag{26}$$

where $g' = dy/dx$, the slope of the body surface. This can be written in the form

$$\psi_n = (\psi_\xi \beta - \psi_\eta \gamma)/(J\gamma^{1/2}) \tag{27}$$

by multiplying numerator and denominator by $x_\xi$.

Thus, from (14)

$$(\psi_\xi \beta - \psi_\eta \gamma)/(J\gamma^{1/2}) = \mathbf{v}_B \cdot \hat{s} \qquad \text{at the body surface.} \tag{28}$$

The numerical scheme for the solution of this problem is essentially that used by Thompson *et al.* [3]. Equation (23) is replaced by a finite-difference approximation through the use of backward time and central space differencing to yield a fully implicit scheme for advancing the vorticity. The resulting equations are solved iteratively in the red–black manner so that latest values can be used in vectorized calculations.

Initially an extension of the explicit DuFort–Frankel scheme previously used successfully on viscous flow problems [14] was tried. However, in the present case a severe limitation on the time step, necessitated by the very small distances between grid points in portions of the flow region, made the scheme unsuitable. When the plates are almost in contact, the region near the vertex tips is overresolved. However, the grid points are needed at later times when the bodies move apart.

The nine-point finite-difference approximation to (16) is solved iteratively using SOR in the red–black manner to achieve vectorization as already discussed for Eq. (3).

The key to a fast iterative method for a time-dependent viscous flow problem is the computation of the vorticity on the boundary. Many schemes use a finite-difference approximation to (24) which incorporates the nonslip condition (28). On the other hand, Israeli [15] proposed a method for applying the nonslip condition directly in an iterative manner. Thompson *et al.* [3] improved upon Israeli's scheme. In any case, relaxation parameters are needed to achieve optimization. In this work both Israeli's method without Thompson's improvement and a scheme based on (24) were employed. Since neither was fully optimized, no conclusions are made concerning their relative efficiency.

The time-advancement proceeds in the following manner:

1. Initial approximations for $\omega_{i,j}^{n+1}$, $\psi_{i,j}^{n+1}$, $\psi_{i,j}'^{n+1}$, $x_{i,j}^{n+1}$, and $y_{i,j}^{n+1}$ are found by linear extrapolation from time levels $n-1$ and $n$.

2. The new locations of grid points on the body surface $(x_{B,j}^{n+1}, y_{B,j}^{n+1})$ are determined, based on the body position at time level $n+1$.

3. Grid point coordinates $(x_{i,j}^{n+1}, y_{i,j}^{n+1})$ are determined by iterating on $x$ and $y$ according to the finite-difference approximation to (3). Since the geometry does not change much in one time step, one or two iterations usually suffice.

4. When necessary, auxiliary stream function values $\psi_{i,j}'^{n+1}$ are determined by iteration according to the finite-difference approximation to (18). Here again one or two iterations is usually sufficient.

5. Interior vorticity values $\omega_{i,j}^{n+1}$ are updated according to (23).

6. Stream function values $\psi_{i,j}^{n+1}$ are updated with one iteration on (24).

7. The vorticity on the boundary $\omega_{B,j}^{n+1}$ is updated so as to enforce (28).

8. Pressure is computed and the proper amount of the auxiliary stream function $\psi'$ is added to $\psi$ so that the corrected pressure is single-valued.

Steps 5–8 are repeated until suitable convergence is achieved. The goal is to handle most of the time advancement by the extrapolation in step 1 so that only a few iterations are needed in the following steps to handle minor corrections.

The results for the opening and closing motion were computed in 210 time steps with $\Delta t = 0.01$. Much larger time increments would most likely lead to very in-

[redacted]

($\omega$ and $\psi$), with a relatively unoptimized version of Israeli's vorticity calculation, was variable but usually less than 100. The flow results were computed with about 5 min of Texas Instruments ASC central processor time.

Figures 6 and 7 display streamlines and lines of constant vorticity at various times for the opening phase of motion. Streamlines of Fig. 6a for $\theta = 11°$ are quite similar to potential flow streamlines except near the bodies. At the bodies the streamlines are tangent to the direction of the body motion in accordance with the nonslip condition. As shown in Fig. 7a, most of the vorticity is generated near the moving tips of the plates. Vorticity is convected into the opening between the plates as the fluid rushes into this gap.

The streamlines at $\theta = 22°$ in Fig. 6b indicate flow separation from the body surfaces at the moving tips. The separation is apparent in the reversal of the velocity component tangential to the body surfaces just behind the tips. Associated with this flow separation are regions of vorticity of sign opposite to that of the vorticity in front of the tips. This vorticity of opposite sign is first noted on the body surfaces, immediately behind the tips at $\theta \simeq 5°$.

The vorticity lines at $\theta = 33°$ (Fig. 7c) show local vorticity extrema away from the body surfaces and hence reveal the shedding of vortices. However, as predicted by Lighthill [9], because of the low Reynolds number and the flow of the fluid into the opening between the plates, significant amounts of vorticity do not travel any great distance from the body surfaces.

Figures 8 and 9 show the closing phase of the motion. At $\theta = 40°$, 31°, and 20° the dissipating vortices generated in the opening phase are still visible. The flow again separates behind the moving tips. In the late stages of the closing a jet develops as fluid is squeezed from between the plates.

In Figs. 10 and 11 results are shown for the plates separating at constant speed after having first opened to $\theta = 45°$. Fluid flows through the growing gap between the plates and vorticity from behind the leading tips is convected into the gap. Once more as predicted by Lighthill [9] a starting vortex such as that shed from the trailing tip of a single airfoil accelerated from rest is not present here. The separating phase was computed in 100 time steps with $\Delta t = 0.01$ using a somewhat optimized body

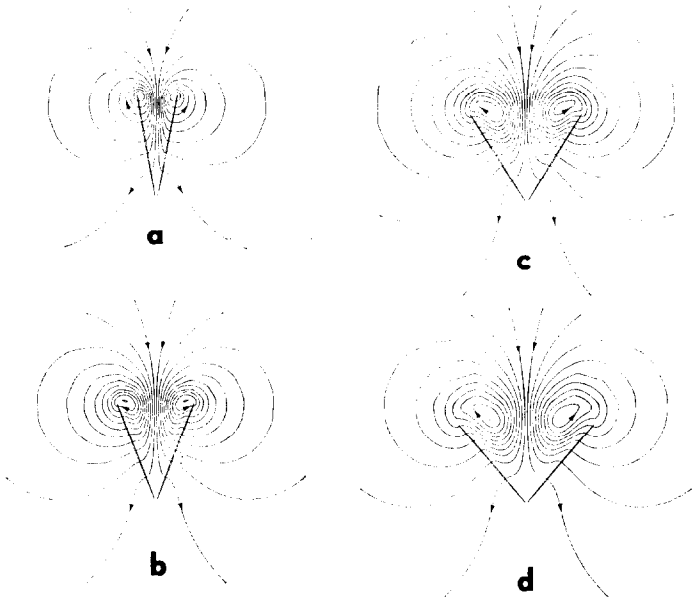


FIG. 6. Sequence of streamlines for the opening phase: (a) $\theta = 11°$, (b) $\theta = 22°$, (c) $\theta = 33°$, (d) $\theta = 41°$.

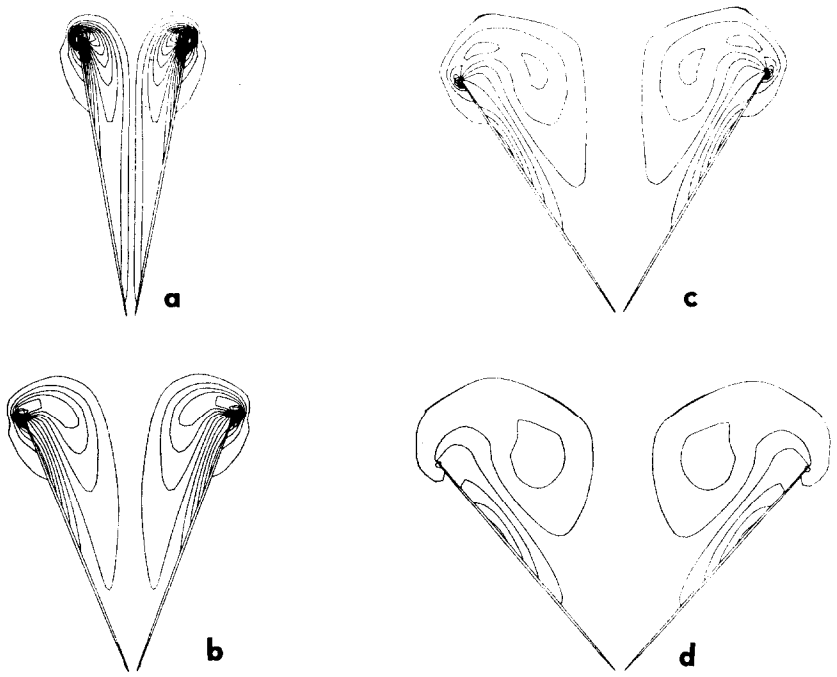


FIG. 7. Sequence of equal-vorticity lines corresponding to the streamlines of Fig. 6.

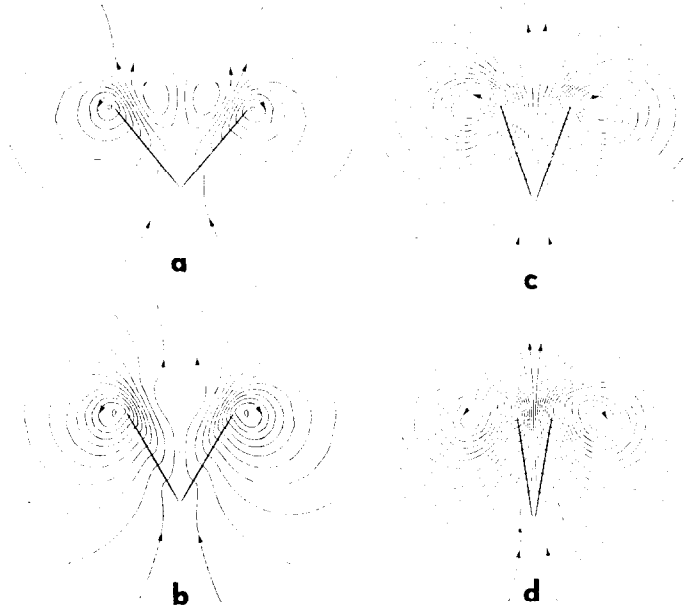


FIG. 8. Sequence of streamlines for the closing phase: (a) $\theta = 40°$, (b) $\theta = 31°$, (c) $\theta = 20°$, (d) $\theta = 9°$.

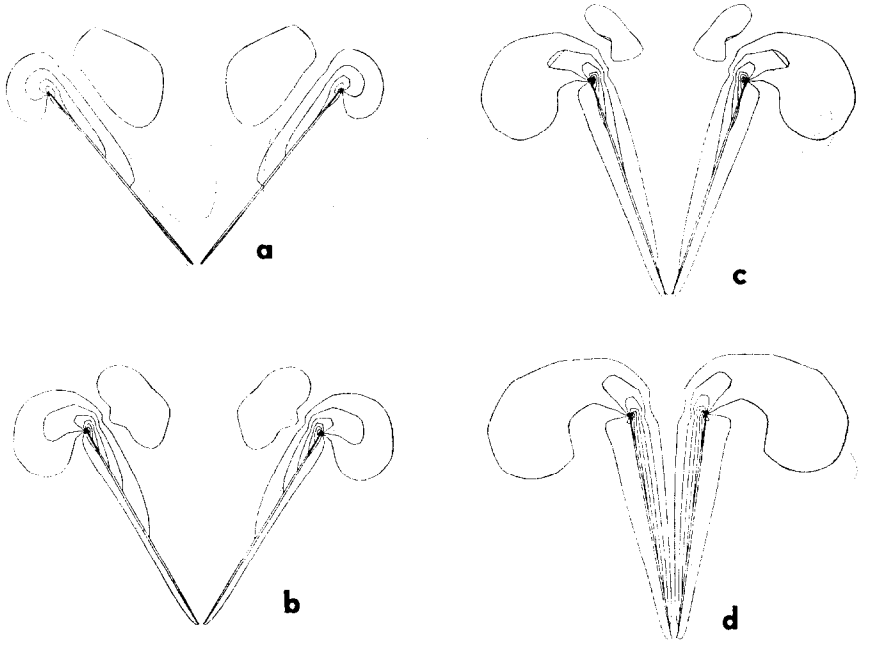


FIG. 9. Sequence of equal-vorticity lines corresponding to the streamlines of Fig. 8.

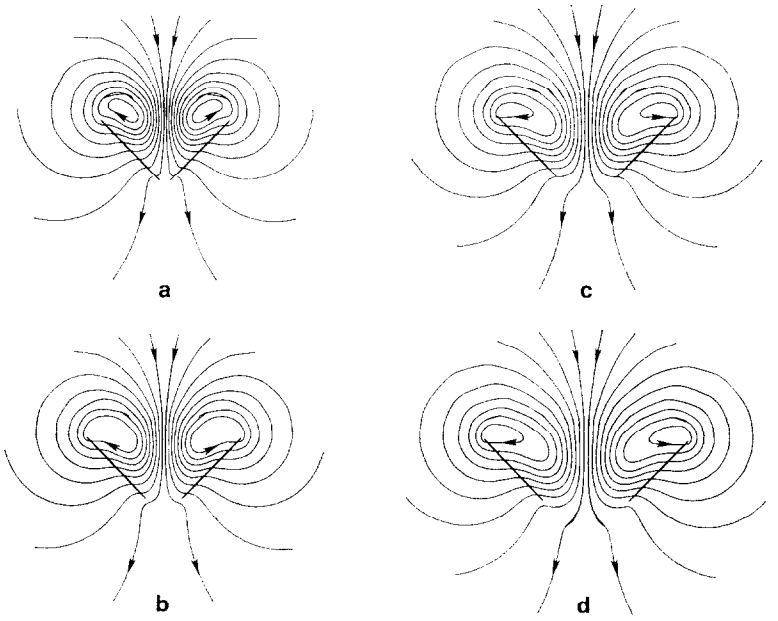


FIG. 10. Sequence of streamlines for the separating phase.

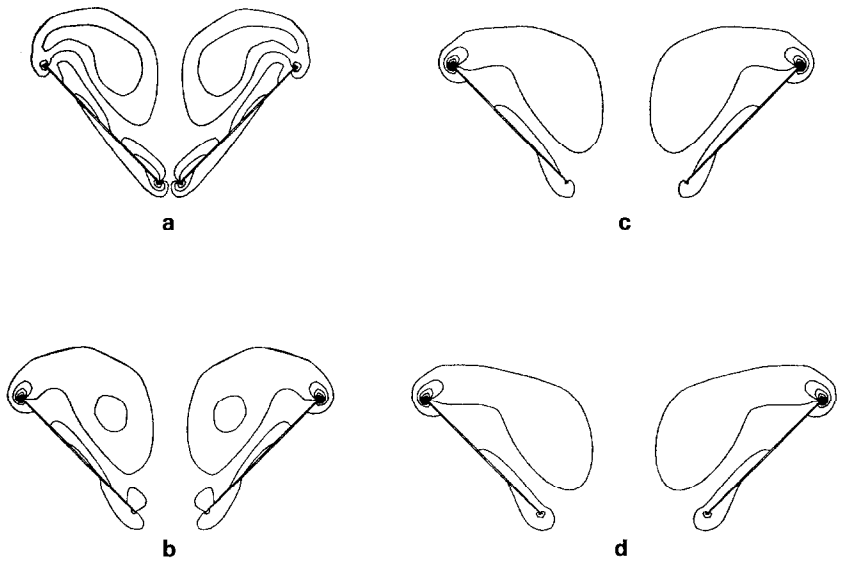


FIG. 11. Sequence of equal-vorticity lines corresponding to the streamlines of Fig. 10.

vorticity calculation based on Eq. (24). The number of iterations per time step averaged about 12 so that even with the extra calculation for the stream function values on the bodies only 43 sec of TI-ASC central processor time was used.

## CONCLUSION

Boundary-fitted coordinate techniques are powerful tools for solving complex flow problems. There is a wide variety in the type of transformations that can be applied. A transformation suitable for multibody problems has been presented and tested successfully on a model for the Weis-Fogh mechanism of lift generation. Such numerical methods, especially when combined with such recent computer technology as high-speed vector processing, allow the accurate solution of flow problems which could not otherwise be tackled.

## ACKNOWLEDGMENTS

The author acknowledges with gratitude the contributions of Mr. R. T. Van Eseltine who programmed the Poisson-solving routines for the TI-ASC and Mr. M. Haas who helped with the graphical display of the meshes and flow fields.

## REFERENCES

1. J. F. THOMPSON, F. C. THAMES, AND C. W. MASTIN, *J. Comp. Phys.* **15** (1974), 299.
2. J. F. THOMPSON *et al.*, Solutions of the Navier–Stokes equations in various flow regimes on fields containing any number of arbitrary bodies using boundary-fitted coordinate systems, *in* "Lecture Notes in Physics" (A. I. van de Vooren and P. J. Zandbergen, Eds.), Vol. 59, p. 421, Springer-Verlag, Berlin/Heidelberg/New York, 1976.
3. J. F. THOMPSON, F. C. THAMES, C. W. MASTIN, AND S. P. SHANKS, Use of numerically generated body-fitted coordinate systems for solution of the Navier-Stokes equations, AIAA Second Computational Fluid Dynamics Conference, Hartford, Conn., 19–20 June 1975.
4. U. GHIA, K. N. GHIA, AND C. J. STUDERUS, Use of surface-oriented coordinates in the numerical simulation of flow in a turbine cascade, *in* "Lecture Notes in Physics" (A. I. van de Vooren and P. J. Zandbergen, Eds.), Vol. 59, p. 197, Springer-Verlag, Berlin/Heidelberg/New York, 1976.
5. H. J. HAUSSLING AND R. M. COLEMAN, Finite-difference computations using boundary-fitted coordinates for free-surface potential flows generated by submerged bodies, Proceedings of the Second International Conference on Numerical Ship Hydrodynamics, Berkeley, Calif., September 1977.
6. J. J. CONNOR AND C. A. BREBBIA, "Finite Element Techniques for Fluid Flow," Newnes–Butterworths, London/Boston, 1976.
7. W. S. LONG, M. S. dissertation, Mississippi State University, Aug. 1977.
8. T. WEIS-FOGH, *J. Exper. Biol.* **59** (1973), 169.
9. M. J. LIGHTHILL, *J. Fluid Mech.* **60** (1973), 1.
10. H. J. LUGT AND S. OHRING, Naval Ship Research and Development Center Report No. 3654, 1971.

11. L. J. H. HAYES, M. S. dissertation, University of Texas at Austin, Aug. 1974.
12. H. J. LUGT AND H. J. HAUSSLING, *J. Appl. Mech.* **45** (1978), 1.
13. D. R. SOOD AND H. G. ELROD, *AIAA J.* **12** (1974), 636.
14. H. J. LUGT AND H. J. HAUSSLING, *J. Fluid Mech.* **65** (1974), 711.
15. M. ISRAELI, *Stud. Appl. Math.* **49** (1970), 327.